A Conformationally Fixed Chiral Bisphosphine Ligand by Steric Modulators on the Ligand Backbone: Selective Synthesis of Strained 1,2-Disubstituted Chiral *cis*-Cyclopropanes

Hiroaki Iwamoto,[†#] Yu Ozawa,[†#] Yuta Hayashi,[†] Tsuneo Imamoto,[†,‡] and Hajime Ito[†,§*]

[†] Division of Applied Chemistry, Graduate School of Engineering, Hokkaido University, Sapporo, Hokkaido 060-8628, Japan

[‡] Department of Chemistry, Graduate School of Science, Chiba University, Yayoi-cho, Inage-ku, Chiba 263-8522, Japan

[§] Institute for Chemical Reaction Design and Discovery (WPI-ICReDD), Hokkaido University Sapporo, Hokkaido 060-8628, Japan

KEYWORDS: cis-Selective asymmetric cyclopropanation, Asymmetric carboboration, Chiral bisphosphine ligand, DFT calculation, Copper(I)-catalysis.

ABSTRACT: A new series of C_1-symmetric P-chirogenic bisphosphine ligands of the type (*R*)-5,8-*Si*-Quinox-*t*Bu$_3$ (*Silyl* = SiMe$_3$, SiEt$_3$, SiMe$_2$Ph) has been developed. The bulky silyl modulators attached to the ligand backbone fix the phosphine substituents to form rigid chiral environments that can be used for substrate recognition. The ligand showed high performances for a copper(I)-catalyzed asymmetric borylative cyclopropanation of bulky silyl-substituted allylic electrophiles to afford higher disfavored 1,2-*cis*-silyl-boryl-cyclopropanes than the other possible isomers, *trans*-cyclopropane and allylboronate (up to 97% yield; 98% ee; *cis*/*trans* = >99:1; cyclopropane/allylboronate = >99:1). Detailed computational studies suggested that the highly rigid phosphine conformation, which is virtually undisturbed by the steric interactions with the bulky silyl-substituted allyl electrophiles, is key to the high stereo- and product-selectivity. Furthermore, the detailed computational analysis provided insight into the mechanism of the stereo-retention or -inversion of the chiral alkylcopper(I) intermediate in the intramolecular cyclization.

INTRODUCTION

Chiral bisphosphines have been recognized as fundamental ancillary ligands in transition-metal-catalyzed reactions as they can bind to the metal and thus help to maintain catalyst activity and establish control over the stereoselectivity.[1–3] Various chiral bisphosphine ligands such as BINAP, Segphos, Josiphos, and DuPhos have been developed and used for the various transformations.[4–10] Modifications of the substituents on the phosphorus atoms represent one major strategy to improve catalyst performance. However, the conformation and steric environment of the catalysts depends not only on the catalyst components, i.e., the ligands and the metal center, but also on the steric and electronic interactions with the substrate. In the case of substrates that bear bulky substituents, steric interactions strongly deform the ideal environment of the ligands to decrease the stereoselectivity.[11,12]

Controlling the ligand conformation in the transition state, where it determines the stereoselectivity, by chiral molecular skeletons and non-covalent interactions can thus be considered a key design concept for chiral ligands.[13–17] We have already introduced steric modulators on the ligand backbone of the P-chirogenic C_2-symmetrical chiral bisphosphine (*R*,*R*)-5,8-*Si*-QuinoxP* to improve the performance of a chiral catalyst (Figure 1a middle).[18] The steric modulators on the ligand backbone can regulate the phosphine conformation to enhance the stereoselectivity and destabilize the dormant species of the catalytic cycle via the steric interactions. Then, we focused on three-hindered-quadrant C_1-symmetrical bisphosphines as their phosphine moieties are sterically more congested than those of the corresponding C_2-symmetrical ligands.[19–23] Such sterically crowded phosphine moieties can be expected to be effectively fixed by the steric modulators on the ligand backbone to create a robust reaction space for stereoselective reactions. Here, we report a new series of C_1-symmetrical chiral bisphosphine ligands of the type (*R*)-5,8-*Si*-Quinox-*t*Bu$_3$, which contain silyl-groups on the ligand backbone (Figure 1a right).

Cyclopropane is one of the most fundamental strained molecular skeletons in organic chemistry.[24–26] Asymmetric synthesis routes to *trans*-cyclopropanes or multi-substituted cyclopropanes based on either chiral transition-metal catalysts including metal-carbenoid intermediates or chiral organocatalysts via intramolecular nucleophilic ring closure have been well established.[27–30] However, the corresponding *cis*-selective asymmetric reactions for vicinal *cis*-1,2-disubstituted cyclopropanes remain challenging due to the high levels of intrinsic strain (Figure 1b).[31–36] Our group

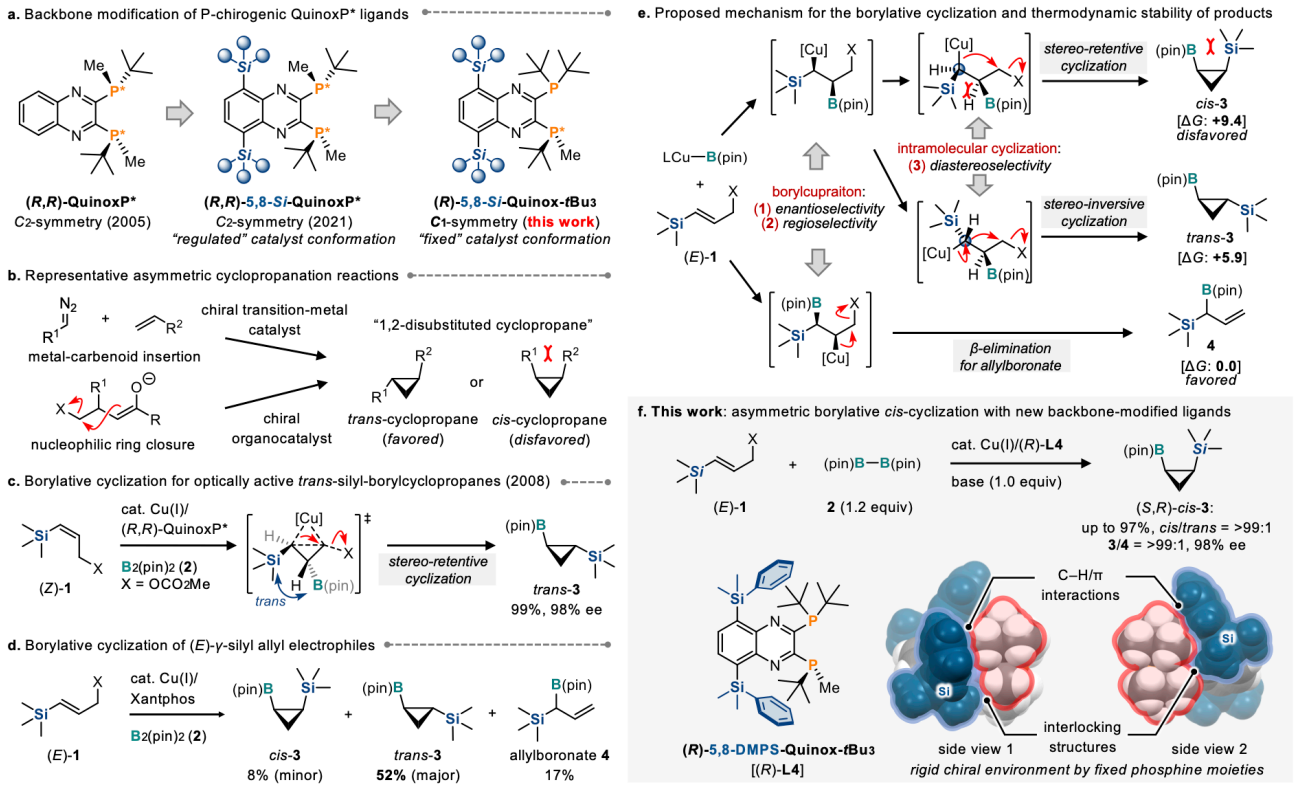

Figure 1. New chiral bisphosphine ligand design and copper(I)-catalyzed stereo- and enantioselective borylative cyclization of highly strained chiral *cis*-1,2-silyl-borylcyclopropanes.

previously reported a copper(I)-catalyzed asymmetric borylative cyclopropanation of (*Z*)-allyl electrophiles to afford *trans*-1,2-functionalized borylcyclopropanes via a stereoretentive intramolecular 3-*exo*-*tet* cyclization (Figure 1c).[37] We thus expected that a similar reaction with (*E*)-allyl electrophiles (*E*)-**1** would furnish the *cis*-cyclopropane *cis*-**3**, which are very useful synthetic blocks for *cis*-cyclopropanes by stereoselective derivatization of the boryl group and silyl group.[38–47] However, contrary to our expectation, the reaction of (*E*)-**1** with the copper(I) catalyst gave a mixture of diastereomers of the cyclopropanes *trans*-**3** and *cis*-**3** as well as allylboronate **4** (Figure 1d). In this cyclopropanation, three different selectivities should be discussed: 1) The enantioselectivity of the borylcupration step; 2) the regioselectivity of the borylcupration step, which determines the product-selectivity between the **3** and **4**; 3) the diastereoselectivity of the intramolecular cyclization step of the alkylcopper(I) intermediate, which can proceed in a stereoretentive or -inversive manner (Figure 1e). The borylative cyclopropanation of (*E*)-**1** showed low selectivity, probably due to the steric congestion in the transition state of the stereo-retentive cyclization. Moreover, according to the thermodynamic stability of the products, the *cis*-cyclopropane, *cis*-**3**, is thermodynamically less stable than its stereoisomer *trans*-**3** and regioisomer **4** due to the highly strained molecular structure, which suggests that the selective formation of *cis*-**3** requires sophisticated kinetic control by the catalyst to overcome the thermodynamic disadvantages (Figure 1e; *cis*-**3**: ΔG = +9.4 kcal/mol; *trans*-**3**: ΔG = +5.9 kcal/mol; **4**: ΔG = 0.0 kcal/mol).[48,49]

Herein, we report backbone-modified C_1-symmetrical ligands of the type (*R*)-5,8-*Si*-Quinox-*t*Bu$_3$, which showed unprecedented *cis*-selectivity and high enantioselectivity in the copper(I)-catalyzed borylative cyclopropanation of (*E*)-alkenyl silanes **1** that bear bulky silyl substituents (Figure 1f; up to 97% yield, 98% ee, *cis*/*trans* = >99:1, **3**/**4** = >99:1). A computational study indicated that the conformational fixation of the phosphine moieties by intramolecular noncovalent interactions with the silyl groups on the backbone generates a rigid chiral environment that enhances the regio- and enantioselectivity. Furthermore, a localized orbital analysis suggested that the intramolecular cyclization proceeds via a nucleophilic attack of the stereogenic carbon atom attached to the copper center in a stereo-retentive manner. During the formation of the minor stereoisomer, the stereoinversion of the stereogenic carbon atom attached to copper can be expected to involve an interaction of the copper(I)–carbon bonding orbital with the *anti*-bonding orbital of the leaving group via an electrophilic substitution (S_E2) mechanism.

RESULTS AND DISCUSSION

First, we investigated the optimal reaction conditions by screening the leaving group of alkenyl silane (*E*)-**1a** as well as various reported chiral bisphosphine ligands (Table 1). The reaction of the (*E*)-allyl carbonate (*E*)-**1aa** with (*R*,*R*)-QuinoxP*, which showed high selectivity for the reaction of (*Z*)-**1aa** in the previous report, furnished a mixture of *cis*- and *trans*-cyclopropanes **3a** and allylboronate **4a** with moderate enantioselectivity for (*S*,*R*)-*cis*-**3a** (Table 1, entry 1).[37] Allyl phosphate (*E*)-**1ab** exhibited higher stereoselectivity than carbonate (*E*)-**1aa** (Table 1, entry 2). The chiral bisphosphine ligand (*R*)-SEGPHOS showed good diastereo- and product-selectivity (**3**/**4**) in the reaction with (*E*)-**1ab**,

albeit that the enantioselectivity was very low (Table 1, entry 3). The use of (*R*)-DTBM-SEGPHOS resulted in low reactivity and enantioselectivity (Table 1, entry 4). Furthermore, a chiral ligand with a planar chirality, (*R*,*S*$_P$)-Josiphos, showed comparable diastereo- and product-selectivity to (*R*,*R*)-QuinoxP*, but poorer enantioselectivity (Table 1, entry 5). We also tested a chiral *N*-heterocyclic carbene (NHC) ligand in this reaction. However, in this case, allylboronate **4a** was obtained in quantitative yield (Table 1, entry 6). Although the various chiral ligands mentioned above exhibited low or moderate stereo- and product-selectivity, we found that the P-chirogenic three-hindered-quadrant bisphosphine ligand (*R*)-Quinox-*t*Bu$_3$ [(*R*)-**L1**] showed higher enantioselectivity and *cis*-selectivity (Table 1, entry 7). However, there was still room for improvement of the enantio- and product-selectivity (**3**/**4**).

Table 1. Initial Investigation of Asymmetric Borylative Cyclopropanation for (*S*,*R*)-*cis*-3a.[a]

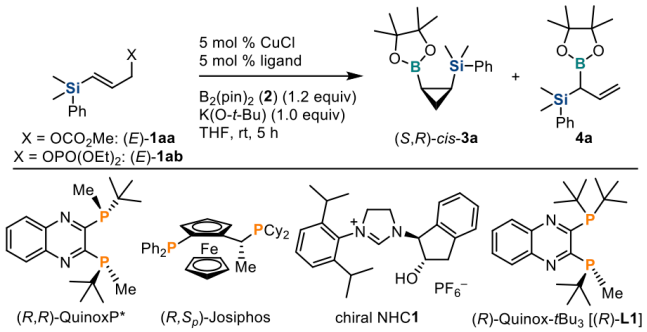

entry	Ligand	**1a**	yield (%)[b]: *cis*-**3a**	ee (%)[c]: *cis*-**3a**	*cis*/*trans*[b]	**3**/**4**[b]
1	(*R*,*R*)-QuinoxP*	(*E*)-**1aa**	35	63	84:16	58:42
2	(*R*,*R*)-QuinoxP*	(*E*)-**1ab**	70	82	91:9	75:25
3	(*R*)-SEGPHOS	(*E*)-**1ab**	72	–11	87:13	89:11
4[d]	(*R*)-DTBM-SEGPHOS	(*E*)-**1ab**	21	43	84:16	35:65
5	(*R*,*S*$_P$)-Josiphos	(*E*)-**1ab**	74	30	91:9	86:14
6	chiral NHC**1**	(*E*)-**1ab**	(98)[e]	(37)[e]	-	<1:99
7	(*R*)-Quinox-*t*Bu$_3$ [(*R*)-**L1**]	(*E*)-**1ab**	86	90	96:4	89:11

[a]Conditions: CuCl (0.025 mmol), ligand (0.025 mmol), (*E*)-**1aa** or (*E*)-**1ab** (0.5 mmol), **2** (0.6 mmol), and K(O-*t*-Bu) (0.5 mmol) in THF (1.0 mL). [b]The yield, diastereoselectivity, and **3**/**4** ratio were determined by ^{1}H NMR analysis using the crude material with an internal standard. [c]The enantioselectivity was determined by HPLC analysis after oxidation of the boryl group of (*S*,*R*)-*cis*-**3a**. [d]Reaction time was 48 h. [e]Yield and enantioselectivity of **4a**.

As proof-of-concept that the steric modulators on the ligand backbone are able to fix the phosphine conformation to improve the selectivities (Figure 1a right), we attempted to modify (*R*)-Quinox-*t*Bu$_3$ [(*R*)-**L1**] via the introduction of bulky silyl groups onto the ligand backbone (Figure 2a).[18] First, the silyl-substituted 2,3-dichloroquinoxaline was prepared using the conditions reported by Knochel and coworkers.[50] The resulting 5,8-disilyl-2,3-dichloroquinoxaline was subjected to a stepwise phosphination/deprotection process with the corresponding achiral and chiral phosphine–borane lithium species. Finally, the corresponding P-chirogenic three-hindered-quadrant bisphosphine ligands that bear steric-modulators on the backbone, i.e., (*R*)-5,8-TMS-Quinox-*t*Bu$_3$ [(*R*)-**L2**; TMS: trimethyl silyl], (*R*)-5,8-TES-Quinox-*t*Bu$_3$ [(*R*)-**L3**; TES: triethyl silyl], and (*R*)-5,8-DMPS-Quinox-*t*Bu$_3$ [(*R*)-**L4**; DMPS: dimethylphenyl silyl] were obtained in moderate to good yield (for details, see the SI).

To understand the steric effects of the silyl groups on the backbone-modified QuinoxP*-type ligands (*R*)-5,8-*Si*-Quinox-*t*Bu$_3$, the X-ray diffraction structures of the ligand molecules and their metal complexes were analyzed (Figures 2b–2d). Single-crystal X-ray diffraction analyses of the ligands (*R*)-5,8-TMS-Quinox-*t*Bu$_3$ [(*R*)-**L2**] and (*R*)-5,8-TES-Quinox-*t*Bu$_3$ [(*R*)-**L3**] were successful (Figures 2b, S4, and S5). The X-ray structure of the TMS-based ligand (*R*)-**L2** indicates that the silyl groups interlock with the phosphine moieties. The steric interactions between the silyl and phosphine groups twist the conformation of the phosphine moieties (orange arrows). Furthermore, the molecular conformation of the TES-group-bearing ligand (*R*)-**L3** is identical to that of (*R*)-**L2** with TMS groups.

Next, to investigate the impact of the silyl groups on the ligand conformation in the metal complex, we carried out a structural analysis of palladium(II) complexes of the ligands (Figure 2c).[51] In contrast to the flat quinoxaline plane of the free ligand (*R*)-**L2** (Figure 2b), the quinoxaline plane in the corresponding palladium complex [(*R*)-**L2**]PdCl$_2$ is twisted. The calculated structure of [(*R*)-**L2**]PdCl$_2$ optimized using density functional theory (DFT) calculations is also in good agreement with the X-ray structure (for details, see Figure S13). Furthermore, the X-ray structure of the palladium complex with the DMPS-based ligand [(*R*)-**L4**]PdCl$_2$ also exhibited a twisted quinoxaline structure and interlocking between the silyl groups and phosphine moieties (Figure 2d). In addition, both phenyl rings of the DMPS groups were located at the same side of the quinoxaline backbone plane to interact with the *tert*-butyl groups on the phosphine moieties through C–H/π-interactions. To obtain information regarding the relative stability of the conformers, we also calculated different conformations for the various palladium(II) complexes in terms of the silyl and phosphine moieties. The twisted conformer with C–H/π-interactions similar to the X-ray structure was also categorized as a favorable conformer among the conformers investigated using DFT calculations (Figure S14). In contrast, for the ligand without the silyl groups, the calculated structure of the palladium complex [(*R*)-**L1**]PdCl$_2$ is a flat structure similar to that of the free ligand (*R*)-**L1** (Figure S13). These comparisons suggest that the silyl group has a strong structure-regulation ability in the metal complexes of the (*R*)-5,8-*Si*-Quinox-*t*Bu$_3$ ligands.

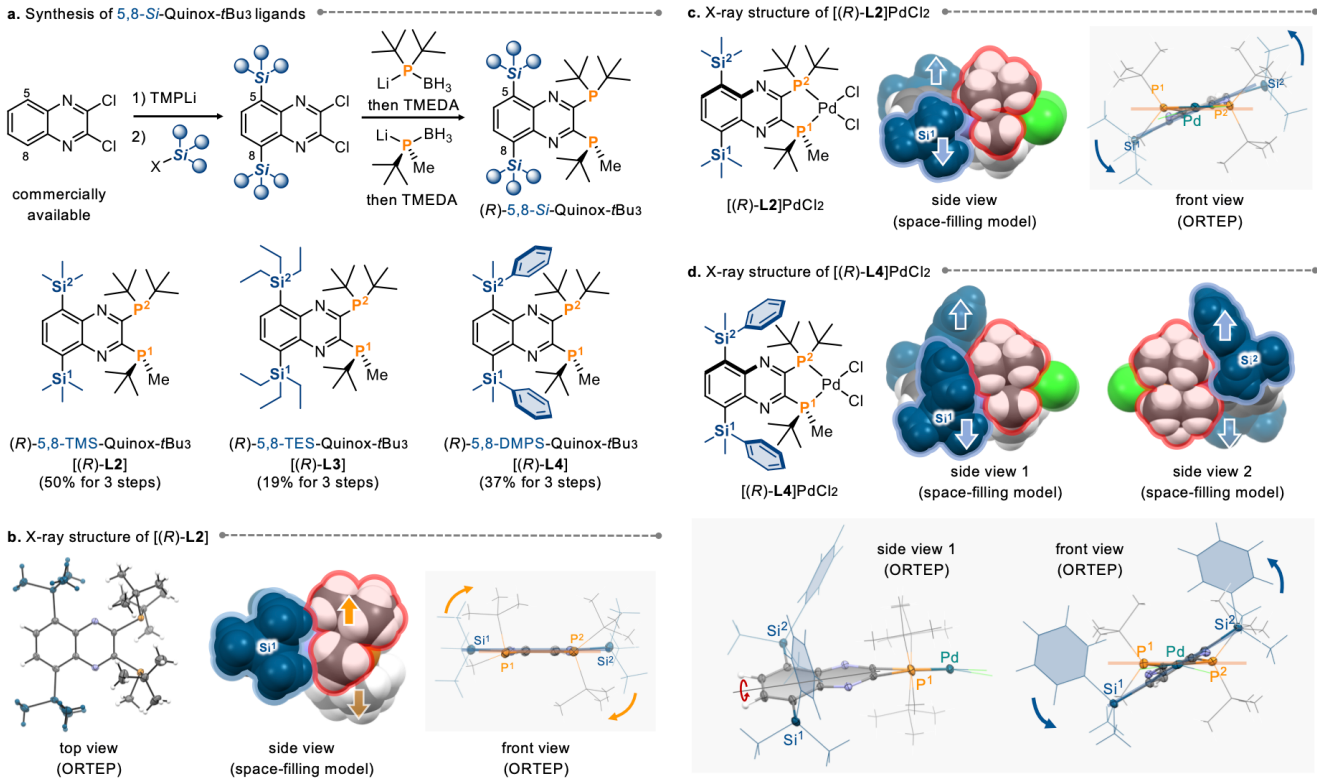

Figure 2. Synthesis and structures of the three-hindered-quadrant chiral bisphosphine ligands modified with sterically demanding silyl modulators, (*R*)-5,8-*Si*-Quinox-*t*Bu$_3$.

Table 2. Asymmetric Borylative Cyclopropanations of Allyl Phosphate (*E*)-1ab with a Series of (*R*)-5,8-*Si*-Quinox-*t*Bu$_3$.[a]

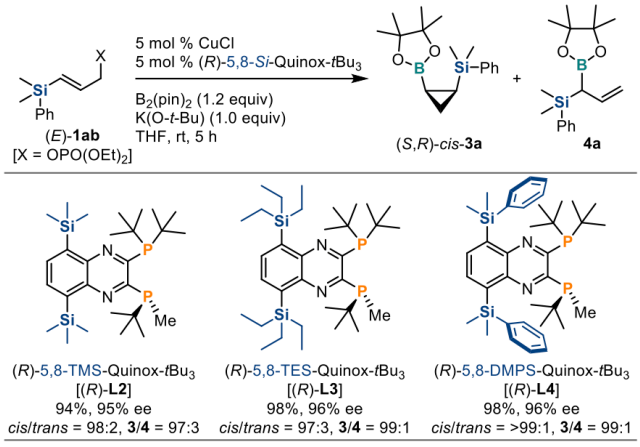

[a]Conditions: CuCl (0.025 mmol), ligand (0.025 mmol), (*E*)-**1ab** (0.5 mmol), **2** (0.6 mmol), and K(O-*t*-Bu) (0.5 mmol) in THF (1.0 mL). The yield, diastereoselectivity, and **3**/**4** ratio were determined by ^{1}H NMR analysis using the crude material with an internal standard. The enantioselectivity was determined by HPLC analysis after oxidation of the boryl group of (*S*,*R*)-*cis*-**3a**.

The new series of (*R*)-5,8-*Si*-Quinox-*t*Bu$_3$ ligands was then tested in the copper(I)-catalyzed asymmetric borylative cyclopropanation of (*E*)-**1ab** (Table 2). The use of (*R*)-**L2** with TMS groups on its backbone enhanced the enantio- and stereoselectivity compared to the ligand without silyl moieties, (*R*)-**L1** [(*R*)-**L2**: 94%, 95% ee, *cis*/*trans* = 98:2, **3**/**4** = 97:3; (*R*)-**L1**: 86%, 90% ee, *cis*/*trans* = 96:4, **3**/**4** = 89:11]. The use of the ligand (*R*)-**L3**, whose TES groups are bulkier steric modulators than the TMS group, slightly improved the selectivities (98%, 96% ee, *cis*/*trans* = 97:3, **3**/**4** = 99:1). Finally, the reaction reached almost perfect stereoselectivity and excellent enantioselectivity to furnish the corresponding *cis*-1,2-silyl-borylcyclopropane (*S*,*R*)-*cis*-**3a** quantitatively when the ligand modified with DMPS groups, [(*R*)-**L4**], was employed (98%, 96% ee, *cis*/*trans* = >99:1, **3**/**4** = 99:1).

Next, we carried out experiments to investigate the substrate scope for the *cis*-selective asymmetric borylative cyclopropanation of allyl electrophiles (*E*)-**1** (Table 3a). The chiral *cis*-1,2-silyl-borylcyclopropane (*S*,*R*)-*cis*-**3a** was isolated in almost quantitative yield with excellent stereoselectivity. The reaction of the allyl phosphate (*E*)-**1bb** bearing a diphenylmethylsilyl group gave the corresponding *cis*-cyclopropane (*S*,*R*)-*cis*-**3b** in excellent yield with almost perfect selectivity. Although the substrate (*E*)-**1cb**, which bears a triphenylsilyl moiety, was smoothly converted into the corresponding cyclopropane (*S*,*R*)-*cis*-**3c** with high reactivity and excellent *cis*-selectivity, the enantioselectivity and product-selectivity were decreased [(*S*,*R*)-*cis*-**3c**: **3**/**4** = 91:9]. Furthermore, the reaction of the allyl phosphate bearing a diphenyl-*tert*-butylsilyl moiety, (*E*)-**1db**, provided a mixture of the cyclopropane **3d** and allylboronate **4d**, but the *cis*/*trans*-selectivity was still high [(*S*,*R*)-*cis*-**3d**: *cis*/*trans* = 96:4]. This reaction system was also applicable to substrates bearing a trialkylsilyl group. The *cis*-cyclopropane (*S*,*R*)-*cis*-**3e** bearing a trimethylsilyl group was obtained in good yield with excellent enantioselectivity when the corresponding allyl carbonate (*E*)-**1ea** was used. In the case of the reactions of substrates that bear trialkyl silyl groups, the use of the phosphates and chlorides slightly decreased the selectivities (Table S3). Although allyl

Table 3. Scope and Applications of the *cis*-Selective Asymmetric Borylative Cyclopropanation of (*E*)-1 with (*R*)-5,8-DMPS-Quinox-*t*Bu$_3$ [(*R*)-L4].

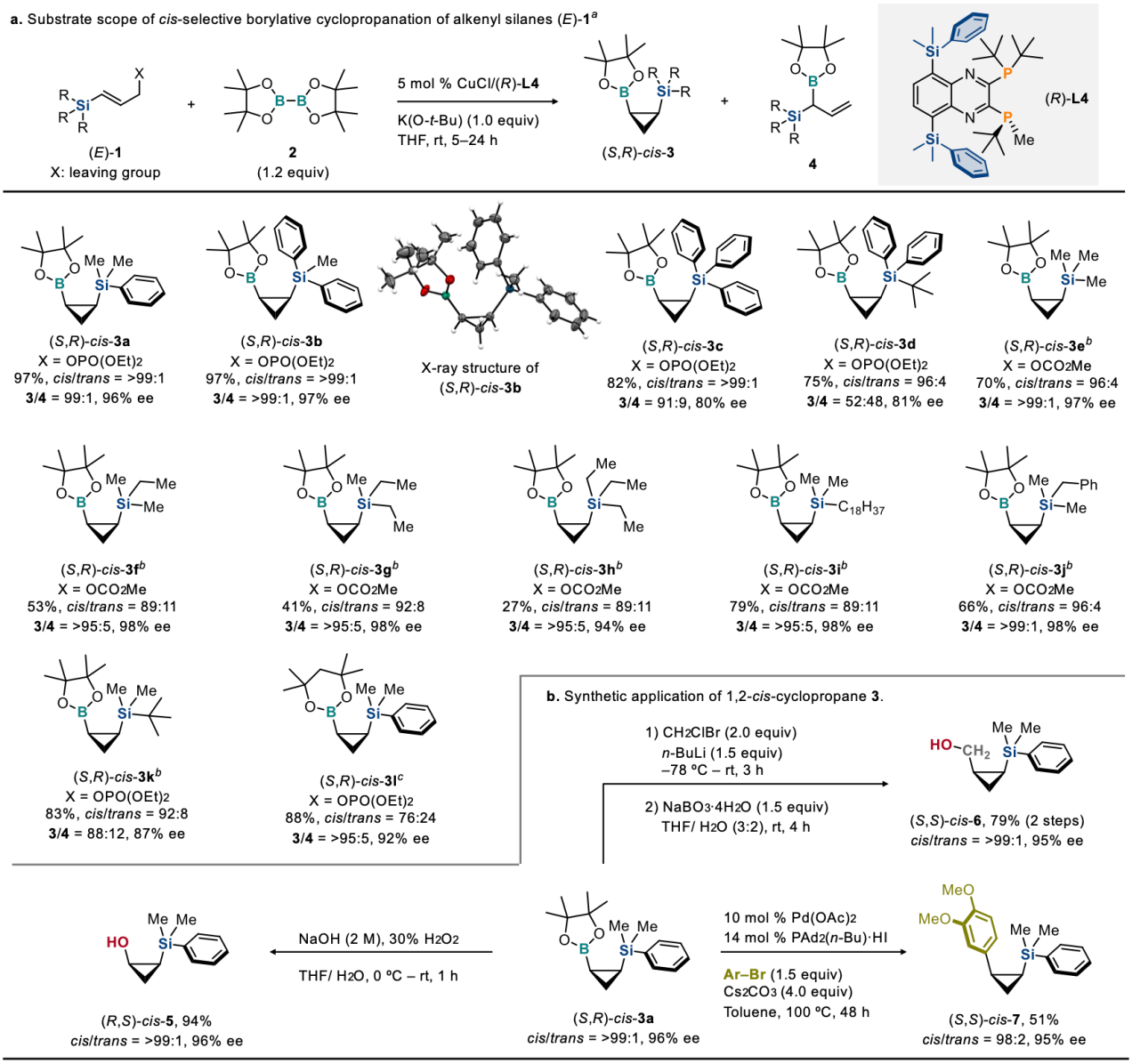

[a]Conditions: CuCl (0.025 mmol), (*R*)-**L4** (0.025 mmol), (*E*)-**1** (0.5 mmol), **2** (0.6 mmol), and K(O-*t*-Bu) (0.5 mmol) in THF (1.0 mL). Isolated yield. The enantioselectivity was determined via HPLC analysis after derivatization of the boryl group of (*S,R*)-*cis*-**3**. The diastereoselectivity (*cis*/*trans*) and product-selectivity (**3**/**4**) were determined via ^{1}H NMR analysis or GC analysis using the crude material. [b]Reaction time: 24 h. [c]Bis(2,4-dimethylpentane-2,4-glycolato)diboron was used instead of **2**.

carbonates with monoethyl- and diethyl-substituted silyl groups, (*E*)-**1fa** and (*E*)-**1ga**, were applicable to the *cis*-selective borylative cyclopropanation [(*S,R*)-*cis*-**3f,** (*S,R*)-*cis*-**3g**], the reaction of the substrate (*E*)-**1ha**, which contains a triethylsilyl moiety, resulted in low reactivity [(*S,R*)-*cis*-**3h**: 27%]. Furthermore, the reaction of an allyl carbonate with a long alkyl chain, (*E*)-**1ia**, also showed high selectivities to provide the corresponding *cis*-cyclopropane (*S,R*)-*cis*-**3i**. The asymmetric cyclopropanation of allyl carbonate (*E*)-**1ja**, which bears a benzyldimethyl silyl moiety, also showed excellent enantioselectivity to provide the corresponding product (*S,R*)-*cis*-**3j** in good yield. Allyl electrophile (*E*)-**1kb**, which contains a bulky trialkylsilyl moiety, was also applicable to the *cis*-selective asymmetric cyclopropanation; the corresponding *cis*-cyclopropane, which bears a *tert*-butyldimethylsilyl moiety, (*S,R*)-*cis*-**3k**, was obtained in high yield with good stereoselectivity. The cyclopropanation of (*E*)-**1ab** using a diboron reagent with a six-membered ring instead of **2** resulted in low diastereoselectivity [(*S,R*)-*cis*-**3l**].

Subsequently, derivatization of the obtained *cis*-silylborylcyclopropane (*S,R*)-*cis*-**3a** was carried out (Table 3b). Oxidation of the boryl group of (*S,R*)-*cis*-**3a** furnished 1,2-*cis*-silylcyclopropanol (*R,S*)-*cis*-**5** in a stereospecific manner (94%, *cis*/*trans* = >99:1, 96% ee). Furthermore, the stepwise derivatization of (*S,R*)-*cis*-**3a** through one-carbon homologation followed by oxidation of the boryl group provided alcohol (*S,S*)-*cis*-**6**, which carries a silylcyclopropane

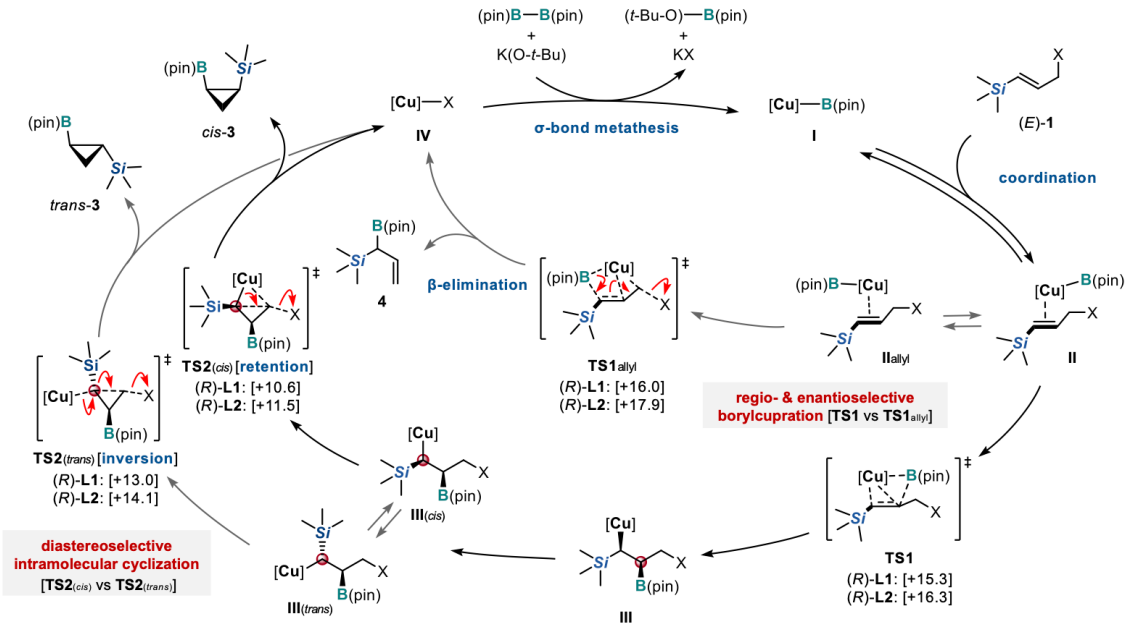

Figure 3. Proposed catalytic cycles for the copper(I)-catalyzed borylative cyclopropanation and allylic borylation.

moiety, with excellent stereospecificity [79% (over 2 steps), *cis*/*trans* = >99:1, 95% ee]. The palladium-catalyzed Suzuki–Miyaura cross-coupling of (*S*,*R*)-*cis*-**3a** with an aryl bromide proceeded to give cyclopropylarene (*S*,*S*)-*cis*-**7** in moderate yield with almost perfect stereospecificity (51%, *cis*/*trans* = 98:2, 95% ee).[45]

A proposed mechanism for the formation of the stereo- and structural isomers (*cis*-**3**, *trans*-**3**, and allylboronate **4**) in this *cis*-selective asymmetric cyclopropanation is shown in Figure 3.[37] First, the reaction between the copper(I) salt and diboron **2** gives the borylcopper(I) active species **I**. Borylcopper(I) **I** and the allyl electrophile (*E*)-**1** then form the π-complex **II**, which is the intermediate for cyclopropane **3**, or regioisomer $\mathbf{II}_{allyl}$, which is the intermediate for allylboronate **4**. The enantioselective borylcupration of **II** via transition state **TS1** provides alkylcopper(I) intermediate **III**, whereas the reaction of $\mathbf{II}_{allyl}$ via the concerted borylation transition state $\mathbf{TS1}_{allyl}$ provides allylboronate **4**.[52] The product-selectivity (**3**/**4**) can be expected to depend on the regioselectivity of the borylcupration at the C–C double bond of (*E*)-**1**, as this step is irreversible. The intramolecular cyclization in a stereo-retentive or -inversive manner, which is the diastereoselectivity-determining step, then proceeds from the corresponding conformers $\mathbf{III}_{(cis)}$ and $\mathbf{III}_{(trans)}$ via transition states $\mathbf{TS2}_{(cis)}$ and $\mathbf{TS2}_{(trans)}$, which lead to *cis*-**3** and *trans*-**3**, respectively. Finally, the corresponding copper(I) salt **IV** would be regenerated.

We then carried out a computational study of the borylcupration step (**TS1**) to understand the mechanism of the enantio- and product-selectivity (**3**/**4**). To simplify the computational study, allyl chloride (*E*)-**1ec**, which bears a trimethyl silyl group, and (*R*)-**L1** or (*R*)-**L2** were employed as the model substrate and ligand for the reaction system in the DFT calculations; these were chosen considering that the experimental results for these reaction systems indicated that (*R*)-**L2** with a TMS-modified backbone showed higher stereoselectivities than the unmodified (*R*)-**L1** [Table S3; (*R*)-**L1**: 94%, 90% ee, *cis*/*trans* = 96:4, **3e**/**4e** = 76:24; (*R*)-**L2**: 95%, 95% ee, *cis*/*trans* = 97:3, **3e**/**4e** = 86:14]. In the case of the addition between an unsymmetrical internal alkene such as (*E*)-**1** and a planar tri-coordinated C_1-symmetrical copper(I) complex with the (*R*)-**L1** or (*R*)-**L2** ligand, at least eight approach patterns of (*E*)-**1** to the metal center should be considered to investigate the regio- and enantioselectivity of the borylcupration.[21] In this work, an exhaustive conformational search of the TSs of the borylcupration, **TS1** and $\mathbf{TS1}_{allyl}$, returned eight transition-state structures for (*R*)-**L1**, and 21 structures for (*R*)-**L2** based on the aforementioned approach patterns (for details, see Figures S19–S21). We selected the TS structures for the borylcupration step with the lowest-energy paths to each of the three isomers, i.e., (*S*,*R*)-*cis*-**3e**, (*R*,*S*)-*cis*-**3e**, and allylboronate **4e**: $\mathbf{TS1}_{major}$ leads to the major enantiomer of the cyclopropane, (*S*,*R*)-*cis*-**3e**; $\mathbf{TS1}_{minor}$ leads to the minor enantiomer of the cyclopropane, (*R*,*S*)-*cis*-**3e**; while $\mathbf{TS1}_{allyl}$ leads to allylboronate **4e**. For both (*R*)-**L1** and (*R*)-**L2**, the DFT calculations indicated that the TSs for the major product (*S*,*R*)-*cis*-**3e** ($\mathbf{TS1}_{major}$) are more favorable than $\mathbf{TS1}_{minor}$ and $\mathbf{TS1}_{allyl}$ [(*R*)-**L1**: $\Delta G^{\ddagger}(\mathbf{TS1}_{major})$ = +15.3 kcal/mol, $\Delta G^{\ddagger}(\mathbf{TS1}_{minor})$ = +16.3 kcal/mol, $\Delta G^{\ddagger}(\mathbf{TS1}_{allyl})$ = +16.0 kcal/mol; (*R*)-**L2**: $\Delta G^{\ddagger}(\mathbf{TS1'}_{major})$ = +16.3 kcal/mol, $\Delta G^{\ddagger}(\mathbf{TS1'}_{minor})$ = +17.7 kcal/mol, $\Delta G^{\ddagger}(\mathbf{TS1'}_{allyl})$ = +17.9 kcal/mol]. Furthermore, the difference between the activation energies ($\Delta\Delta G^{\ddagger}$) of $\mathbf{TS1}_{major}$ and $\mathbf{TS1}_{minor}$ for silyl-group-modified (*R*)-**L2** was slightly larger than that for (*R*)-**L1** without the silyl groups [(*R*)-**L1**: $\Delta\Delta G^{\ddagger}$ = $\Delta G^{\ddagger}$(16.31)–$\Delta G^{\ddagger}$(15.32) = +1.0 kcal/mol; (*R*)-**L2**: $\Delta\Delta G^{\ddagger}$ = $\Delta G^{\ddagger}$(17.68)–$\Delta G^{\ddagger}$(16.34) = +1.3 kcal/mol]. This is consistent with the experimental results, in which the silyl group-modified ligand (*R*)-**L2** showed slightly higher enantioselectivity than (*R*)-**L1** [(*R*)-**L1**: 90% ee; (*R*)-**L2**: 95% ee]. Additionally, the difference between the activation energies of $\mathbf{TS1}_{major}$ and $\mathbf{TS1}_{allyl}$ using (*R*)-**L2** was also larger than that with (*R*)-**L1** [(*R*)-**L1**: $\Delta\Delta G^{\ddagger}$ = $\Delta G^{\ddagger}$(16.02)– $\Delta G^{\ddagger}$(15.32) = +0.7 kcal/mol; (*R*)-**L2**: $\Delta\Delta G^{\ddagger}$ = $\Delta G^{\ddagger}$(17.89)– $\Delta G^{\ddagger}$(16.34) = +1.6 kcal/mol]. This result is also consistent with the experimental results

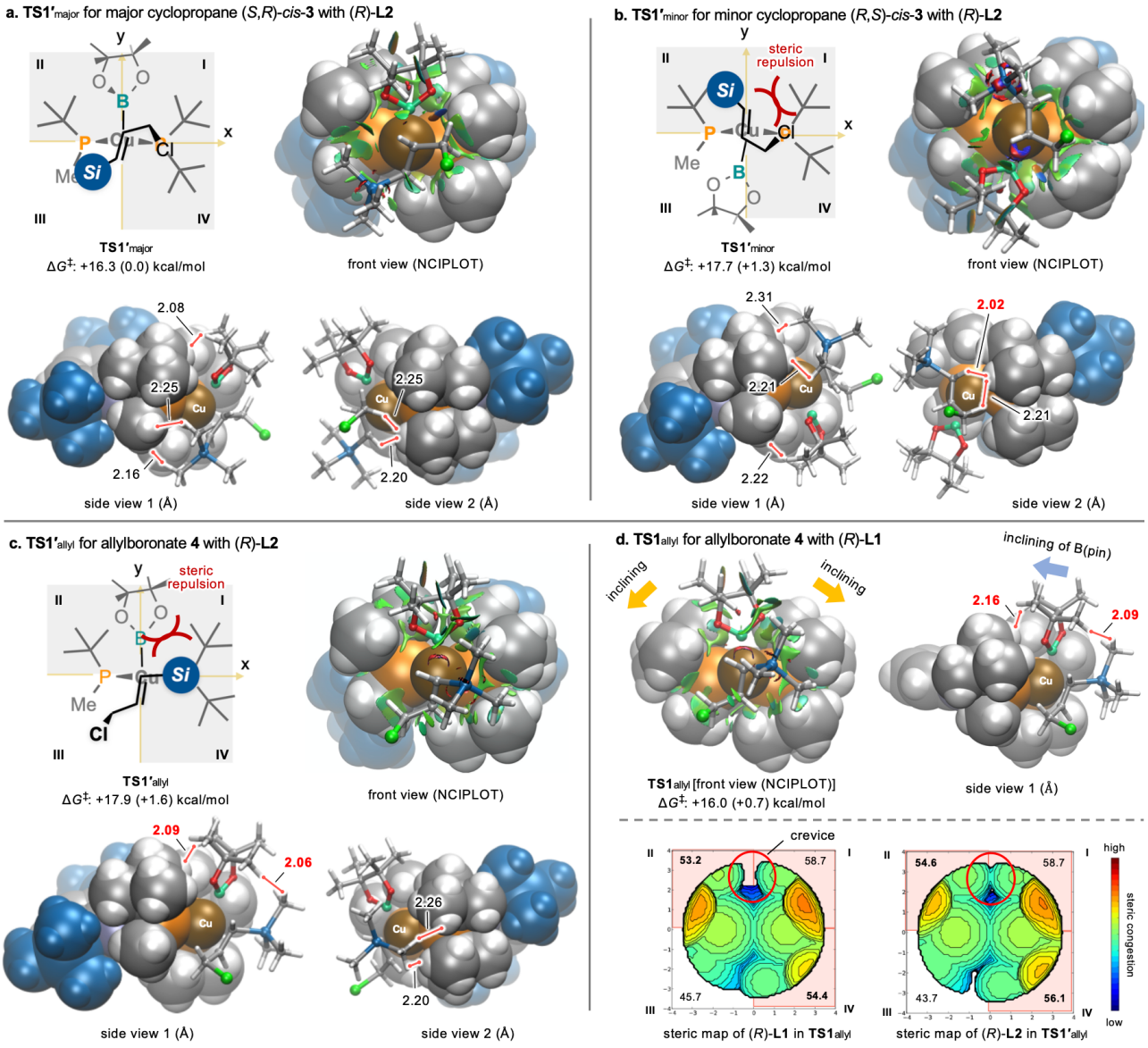

Figure 4. DFT calculations for the asymmetric borylation of allyl chloride (*E*)-**1ec** with (*R*)-**L1** and (*R*)-**L2**. Relative Gibbs energy values [Δ*G* (kcal/mol)] were calculated at the ωB97X-D/Def2-TZVP/SMD(THF)//ωB97X-D/Def2-SVP/SMD(THF) level of theory. Steric maps represent the three-dimensional topography of the phosphine ligands from the perspective of the copper(I)-center in the corresponding transition states.

of (*E*)-**1ec**, in which (*R*)-**L2** showed higher product-selectivity between cyclopropane **3** and allylboronate **4** [(*R*)-**L1**: **3**/**4** = 76:24; (*R*)-**L2**: **3**/**4** = 86:14].[53]

Then, a structural analysis of the important TSs using NCIPLOT[54] was carried out to understand the enantioselectivity and regioselectivity of the borylcupration step (Figure 4). In the most stable **TS1′**$_{major}$, the silyl group of the substrate (*E*)-**1e** is located in the less hindered quadrant **III**. The NCIPLOT of the structure of **TS1′**$_{major}$ indicates a small isosurface of steric contacts between the silyl moiety of (*E*)-**1e** and the phosphine substituent in quadrant **III**. This result suggests that the conformation minimizes the steric repulsions between the catalyst and substrate (Figure 4a). Conversely, the TS structure of **TS1′**$_{minor}$ contains a short contact between the hydrogen atom of the phosphine substituent in quadrant **I** and the hydrogen atom at the vinyl position of the substrate (Figure 4b, distance between these hydrogen atoms: 2.02 Å). This sterically congested structure would be caused by a horizontal shift of (*E*)-**1e** in X-axial direction in order to avoid the steric contact between the silyl group of (*E*)-**1e** and the phosphine substituent in quadrant **II**. The NCIPLOT-derived steric contact isosurface also displays these steric interactions in quadrants **I** and **II**. Therefore, the mismatched structure destabilizes **TS1′**$_{minor}$ more than **TS1′**$_{major}$.

We also conducted the NCIPLOT analysis for the TSs for the formation of the allylboronate **4**. The structure of **TS1′**$_{allyl}$ would be destabilized by the steric repulsion between the B(pin) moiety and the silyl group of (*E*)-**1e** considering the steric contact that should result from the very contact of these hydrogen atoms in these moieties (Figure 4c, distance between these hydrogen atoms: 2.06 Å). Moreover, an increased isosurface between the B(pin) moiety and the silyl-moiety of (*E*)-**1e** was observed in the

NCIPLOT of **TS1′**$_{allyl}$. In previous studies, the regioselectivity toward the formation of borylcyclopropanes, in which the copper(I) atom must attach to the carbon atom adjacent to the silicon atom in the alkenyl silane substrate, was rationalized in terms of the stabilizing electronic effect of the silyl group on the newly formed Cu–C bond.[37,55–57] However, we found that the steric contacts between the substrate and the phosphine substituents of the ligands also crucially affect the regioselectivity.

To investigate the difference of regioselectivity between the silyl-modified ligand (*R*)-**L2** and the original ligand (*R*)-**L1**, we compared the TS structures of **TS1**$_{allyl}$. The result of the structural analysis of **TS1**$_{allyl}$ with (*R*)-**L1** is shown in Figure 4d. The NCIPLOT-derived isosurface area of **TS1**$_{allyl}$ is smaller than that of **TS1′**$_{allyl}$. Furthermore, the distances between the hydrogen atoms in the B(pin) moiety and those of the phosphine substituents or the silyl moiety of (*E*)-**1e** in **TS1**$_{allyl}$ with (*R*)-**L1** are longer than those of **TS1′**$_{allyl}$ with (*R*)-**L2** [H(B(pin))–H(substrate), (*R*)-**L1**: 2.09 Å, (*R*)-**L2**: 2.06 Å; H(ligand)–H(B(pin)), (*R*)-**L1**: 2.16 Å, (*R*)-**L2**: 2.09 Å]. This result indicates that these steric interactions are smaller in **TS1**$_{allyl}$ with (*R*)-**L1** than those in **TS1'**$_{allyl}$ with (*R*)-**L2**. This promotes the formation of the undesired allylboronate isomer **4**. To visualize the phosphine conformation of the ligands in the TSs, steric maps of **TS1**$_{allyl}$ [(*R*)-**L1**] and **TS1′**$_{allyl}$ [(*R*)-**L2**] were obtained using the *SambVca* 2.1 web application (Figure 4d, bottom).[58,59] The steric map of **TS1**$_{allyl}$ displays a steric crevice between quadrants **I** and **II**, where the B(pin) moiety is located. This structure shows that the phosphine substituents in quadrants **I** and **II** incline to the equatorial plane to avoid the steric interactions with the B(pin) moiety. This inclined phosphine conformation would reduce the steric repulsion between the B(pin) moiety and the silyl moiety of the substrate to decrease the activation energy barrier of **TS1**$_{allyl}$. Conversely, no crevice is present in the steric map of **TS1′**$_{allyl}$ because the phosphine substituents and the adjacent silyl groups on the ligand backbone push each other up/down, thus fixing the ligand structure (Figure 4c bottom). Therefore, the silyl group-supported robust structure of (*R*)-**L2** effectively prevents the conformational relaxation to decrease the steric repulsion between the B(pin) and the silyl-moiety of the substrate, which enhances the regioselectivity of the borylcupration.[60]

We also confirmed the advantages of the C_1-symmetric QuinoxP*-type ligands compared to the C_2-symmetric ligand (*R*,*R*)-QuinoxP* for the stereoselectivity of this reaction system (Figure S22). In the C_2-symmetric ligand, quadrant **I** is less hindered than in the C_1-symmetric ligand because the *tert*-butyl group in quadrant **I** is replaced by a methyl group. Therefore, the steric repulsion in quadrant **I** of the transition states for the minor enantiomer (**TS1'**$_{minor}$ and **TS1'**$_{allyl}$) can be expected to be reduced, which would decrease the activation-energy barriers of these minor reaction pathways. In fact, the enantio- and product-selectivity of the reaction using (*R*,*R*)-QuinoxP* were lower than those of the reaction using the C_1-symmetric QuinoxP*-type ligand (*R*)-**L1** (Table 1, S2, and S3).

Next, we focused on the mechanism of the intramolecular cyclization step [**TS2** with (*R*)-**L1**] from the alkylcopper(I) intermediates **III**$_{major}$ or **III**$_{minor}$ to the cyclopropane products **3** (Figure 5).[61] There are four possible reaction routes based on the diastereoselectivity for each diastereomer of **III**$_{major}$ and **III**$_{minor}$: 1) **TS2**$_{major(cis)}$ leads to the major product (*S*,*R*)-*cis*-**3** in a stereo-retentive manner; 2) **TS2**$_{major(trans)}$ leads to the *trans*-cyclopropane (*R*,*R*)-*trans*-**3** in a stereo-inversive manner; 3) **TS2**$_{minor(cis)}$ leads to the minor enantiomer (*R*,*S*)-*cis*-**3** in a stereo-retentive manner; and 4) **TS2**$_{minor(trans)}$ leads to the *trans*-cyclopropane (*S*,*S*)-*trans*-**3** in a stereo-inversive manner (Figure 5a). An energetic analysis of these intramolecular cyclization pathways was conducted using DFT calculations (Figure 5b).[62] In the intramolecular cyclization of **III**$_{major}$, the activation energy for the stereo-retentive pathway via **TS2**$_{major(cis)}$, which provides the desired (*S*,*R*)-*cis*-**3**, is lower than that via the stereo-inversive **TS2**$_{major(trans)}$, which provides the undesired (*R*,*R*)-*trans*-**3** [**TS2**$_{major(cis)}$: $\Delta G^{\ddagger}$ = +10.6 kcal/mol; **TS2**$_{major(trans)}$: $\Delta G^{\ddagger}$ = +13.0 kcal/mol]. Likewise, in the case of the intramolecular cyclization of the alkylcopper(I) intermediate **III**$_{minor}$, **TS2**$_{minor(cis)}$ leads to the undesired enantiomer of the *cis* product, (*R*,*S*)-*cis*-**3**, and the pathway via **TS2**$_{minor(cis)}$ is more favorable than that via **TS2**$_{minor(trans)}$, which leads to the *trans* product (*S*,*S*)-*trans*-**3** [**TS2**$_{minor(cis)}$: $\Delta G^{\ddagger}$ = +11.7 kcal/mol; **TS2** $_{minor(trans)}$: $\Delta G^{\ddagger}$ = +12.6 kcal/mol]. The energy difference between **TS2**$_{major(cis)}$ and **TS2**$_{major(trans)}$ is larger than that between **TS2**$_{minor(cis)}$ and **TS2**$_{minor(trans)}$, thus favoring the formation of the *cis* product (*S*,*R*)-*cis*-**3** in the cyclization step from **III**$_{major}$ compared to the cyclization from **III**$_{minor}$ [**TS2**$_{major(cis)}$ vs **TS2**$_{major(trans)}$: $\Delta\Delta G^{\ddagger}$ = +2.4 kcal/mol; **TS2**$_{minor(cis)}$ vs **TS2**$_{minor(trans)}$: $\Delta\Delta G^{\ddagger}$ = +0.9 kcal/mol]. This analysis indicates that the *cis*/*trans* selectivities of the cyclization step from the alkylcopper(I) intermediates **III**$_{major}$ and **III**$_{minor}$ are different. Furthermore, this diastereomer-dependent stereoselectivity can be considered a partial kinetic resolution that affects the enantioselectivity of the *cis*-**3** and *trans*-**3** products. In fact, the experimental results of the reaction of (*E*)-**1e** showed that the *cis*-**3e** product exhibited high enantioselectivity, while the enantioselectivity of *trans*-**3e** was significantly lower (Table S3; *cis*-**3e**: 90% ee, *trans*-**3e**: 46% ee). The calculation results were in moderate agreement with the experimental results, as the estimated enantioselectivity of the *cis* product *cis*-**3e** was significantly higher than that of the *trans* product *trans*-**3e**, although the predicted ee values (ee$_{pre}$) were slightly underestimated (ee$_{pre}$ for *cis*-**3e**: 74% ee; ee$_{pre}$ for *trans*-**3e**: –36% ee). Furthermore, the diastereoselectivity predicted by the DFT calculations was in good agreement with the experimentally observed diastereoselectivity (calculation: *cis*/*trans* = 95:5; experiment: *cis*/*trans* = 96:4).

Additional DFT calculations using a sterically less congested ligand, (*R*,*R*)-QuinoxP*, for comparison suggested that the high *cis*-selectivity was enhanced by the steric congestion between the silyl or boryl groups and the bulky alkyl groups of three-hindered-quadrant bisphosphine ligands (for details, see Figure S27). This is consistent with the experimental result, in which the use of (*R*,*R*)-QuinoxP* resulted in lower diastereoselectivity [(*R*,*R*)-QuinoxP*: *cis*/*trans* = 88:12; for details, see Table S3].

In addition, we also considered the possibility of another conceivable reaction pathway to access the *trans*-product, *trans*-**3**, in a stereo-inversive manner. Recently, β-hydride

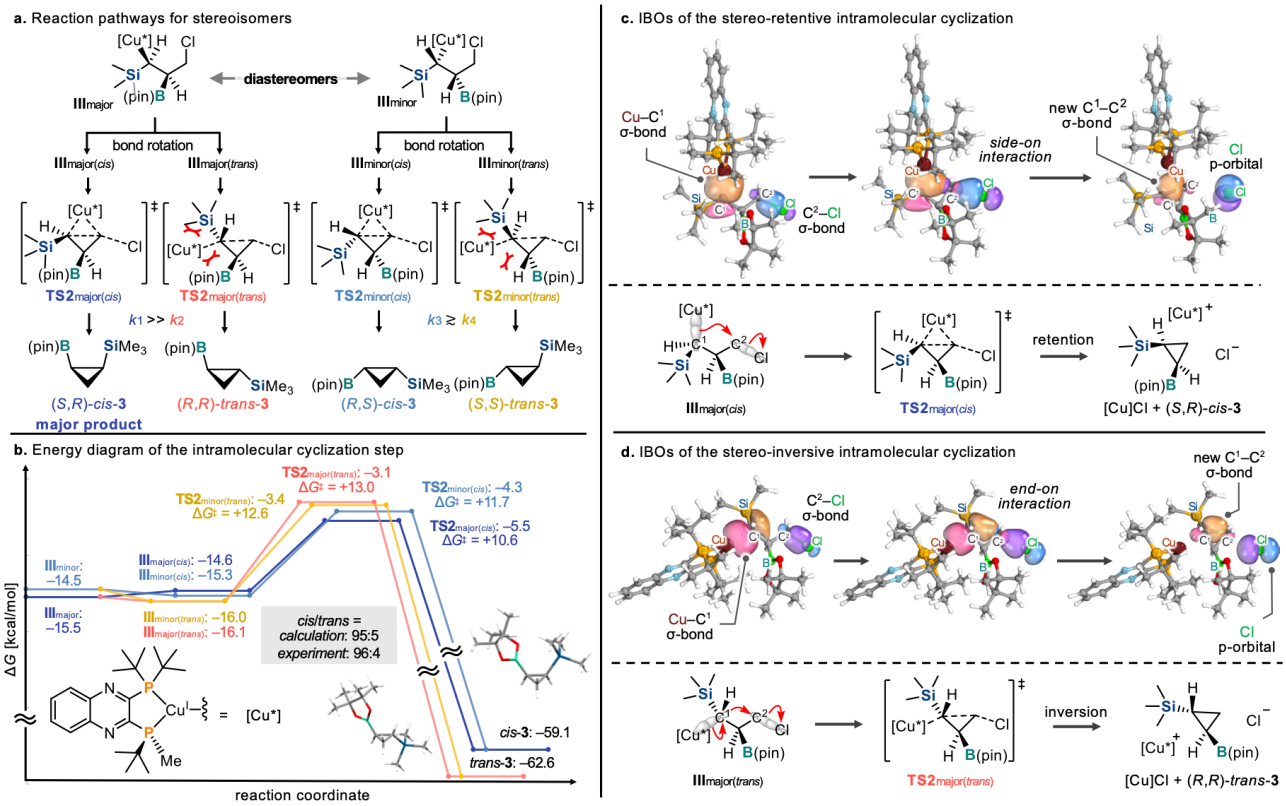

Figure 5. Analysis of the intramolecular cyclization to give cyclopropane **3** using DFT calculations and an intrinsic bonding orbital (IBO) analysis. Relative Gibbs energy values [ΔG (kcal/mol)] were calculated at the ωB97X-D/Def2-TZVP/SMD(THF)//ωB97X-D/Def2-SVP/SMD(THF) level of theory.

elimination from alkylcopper(I) species followed by reinsertion of the copper(I) hydride Cu(I)–H to the alkene has been proposed as an epimerization mechanism of alkylcopper(I) intermediates.[63,64] In our reaction, the relative energy of the TS of the β-hydride elimination of the alkylcopper(I) intermediate **III**$_{major}$ was significantly higher than those of the intramolecular cyclization pathways for the *cis*- and *trans*-products [β-H elimination: $\Delta G^{\ddagger}$ = +25.4 kcal/mol; **TS2**$_{major(cis)}$: $\Delta G^{\ddagger}$ = +10.6 kcal/mol; **TS2**$_{major(trans)}$: $\Delta G^{\ddagger}$ = +13.0 kcal/mol; for details, see Figure S15]. Therefore, the epimerization pathway via β-H elimination was ruled out.

Subsequently, we conducted further investigations in order to understand the mechanism of the intramolecular cyclization step in detail (Figure 5c and 5d). It is known that the nucleophilic C–C-bond formation of alkylcopper(I) species proceeds through an oxidative addition that involves a copper(III) intermediate.[65] However, our computational study did not output a mechanism through the corresponding copper(III) metallacycle. The detailed mechanism of C–C-bond formation from the stereogenic alkylcopper(I) intermediate in both a stereo-retentive and -inversive manner remains elusive.[66] To reveal the details of the TSs of the intramolecular cyclization (**TS2**), we employed an intrinsic bonding orbital (IBO) analysis, which can connect the actual electron flow along the intrinsic reaction coordinate (IRC) with the classical curved arrow formalism.[67,68] An analysis of the intramolecular cyclization from the alkylcopper(I) intermediates **III**$_{major(cis)}$ or **III**$_{major(trans)}$ to the cyclopropanes (*S*,*R*)-*cis*-**3e** or (*R*,*R*)-*trans*-**3e** indicated that the nature of the IBOs of the Cu–C^1 and C^2–Cl σ-bonds changes during the formation of the C^1–C^2 bond and a lone pair of the chloride anion. In the case of the *cis*-selective stereo-retentive cyclization, the IBOs suggested that the electrons of the Cu–C^1 σ-orbital would attack the C^2–Cl σ*-orbital with a side-on interaction mode and the electrons of the C^2–Cl σ-orbital would become a lone pair of a chloride anion (Figure 5c). This process can be recognized as a combination of a nucleophilic substitution (S_N2) at the carbon center (C^2) attached to the chlorine atom and a stereo-retentive electrophilic substitution (S_E2) at the carbon center (C^1) attached to the copper(I) center. In the *trans*-cyclization, the analysis suggested that the electrons of the Cu–C^1 bond would attack the chloride moiety with an end-on interaction mode using the lobe of the Cu–C^1 σ-orbital opposite to the bonding direction (Figure 5d). This bond formation should be possible because the electron occupancy of the opposite lobe of the Cu–C^1 bond would be sufficiently large to interact with the electrophilic moiety. This process could be recognized as a stereo-inversive electrophilic substitution (S_E2) at the carbon center (C^1) attached to the copper(I) center.[69] Therefore, the stereogenic alkylcopper(I) might react with various electrophiles in both stereo-retentive and -inversive manners. This can also explain our previous results involving varied cyclization selectivities.[37]

CONCLUSION

In summary, we have developed the silyl-modified three-hindered-quadrant QuinoxP*-type ligands (*R*)-5,8-*Si*-Quinox-*t*Bu$_3$. By taking advantage of the silyl-modulators on the ligand backbone, we accomplished unprecedentedly

high selectivities for the copper(I)-catalyzed asymmetric *cis*-selective borylative cyclopropanation of allyl electrophiles that bear a bulky silyl group to give highly strained cyclopropane derivatives. Among the corresponding cyclopropane isomers **3** and allylboronate **4**, this reaction can furnish the most strained product, 1,2-*cis*-silyl-boryl-cyclopropanes **3** (up to 97%, 98% ee, *cis*/*trans* = >99:1, **3**/**4** = >99:1). Computational studies indicated that the highly rigid chiral environment of the backbone-modified ligand, which is not affected by the steric interactions with the allyl electrophiles that bear a bulky silyl substituent, is important for the high enantioselectivity and regioselectivity. Furthermore, the DFT and IBO studies shed light on the mechanism of the intramolecular cyclization steps of the stereo-defined alkylcopper(I) intermediates. These steps can be expected to proceed via concerted substitution mechanisms with stereo-retentive and -inversive manners from the same intermediate rather than through the epimerization of the stereo-defined copper(I)–carbon bond via β-H elimination. Efforts to apply this new series of chiral, three-hindered-quadrant bisphosphine ligands to other enantioselective reactions are currently in progress in our laboratory.

ASSOCIATED CONTENT

Supporting Information

The Supporting Information is available free of charge on the ACS Publications website.
Experimental procedure, compound characterization, NMR spectra, and computational data (PDF)
X-ray crystallography data (CIF)
Calculated structures (ZIP)

AUTHOR INFORMATION

Corresponding Author

* hajito@eng.hokudai.ac.jp

Author Contributions

The manuscript was written through contributions of all authors. All authors have given approval to the final version of the manuscript. #These authors contributed equally.

ACKNOWLEDGMENT

This work was financially supported by the Institute for Chemical Reaction Design and Discovery (WPI-ICReDD), which was established by the World Premier International Research Initiative (WPI), MEXT, Japan, as well as by JSPS KAKENHI grants 17H06370 and 18H03907. H. Iwamoto would like to thank the JSPS for a scholarship (16J01410). Y. O. would like to thank the JSPS for a scholarship (19J20823) and the "Program for Leading Graduate Schools" (Hokkaido University "Ambitious Leaders Program"). We thank Dr. Tomohiro Seki, Dr. Mingoo Jin, Mr. Koh Kobayashi and Mr. Kentaro Ida for the X-ray analysis. Parts of the computational calculations were carried out on the supercomputer of Research Center for Computational Science, Okazaki, Japan.

REFERENCES

1) *Phosphorus ligands in asymmetric catalysis: Synthesis and application*; Börner, A., Ed.; Wiley-VCH: Weinheim, 2008; Vol. *1–3*.
2) *Phosphorus(III) ligands in homogeneous catalysis design and synthesis*; Kamer, P. C. J., van Leeuwen, P. W. N. M., Eds.; Wiley-VCH: Weinheim, 2012.
3) Tang, W.; Zhang, X. New chiral phosphorus ligands for enantioselective hydrogenation. *Chem. Rev.* **2003**, *103*, 3029–3069.
4) Noyori, R. Asymmetric catalysis: Science and opportunities (Nobel Lecture). *Angew. Chem., Int. Ed.* **2002**, *41*, 2008–2022.
5) Berthod, M.; Mignani, G.; Woodward, G.; Lemaire, M. Modified BINAP: The how and the why. *Chem. Rev.* **2005**, *105*, 1801–1836.
6) Shimizu, H.; Nagasaki, I.; Matsumura, K.; Sayo, N.; Saito, T. Developments in asymmetric hydrogenation from an industrial perspective. *Acc. Chem. Res.* **2007**, *40*, 1385–1393.
7) Burk, M. J. Modular phospholane ligands in asymmetric catalysis. *Acc. Chem. Res.* **2000**, *33*, 363–372.
8) Gómez Arrayás, R.; Adrio, J.; Carretero, J. C. Recent applications of chiral ferrocene ligands in asymmetric catalysis. *Angew. Chem., Int. Ed.* **2006**, *45*, 7674–7715.
9) Knowles, W. S. Asymmetric hydrogenations (Nobel Lecture). *Angew. Chem., Int. Ed.* **2002**, *41*, 1998–2007.
10) Imamoto, T. Searching for practically useful P-chirogenic phosphine ligands. *Chem. Rec.* **2016**, *16*, 2659–2673.
11) Lu, G.; Fang, C.; Xu, T.; Dong, G.; Liu, P. Computational study of Rh-catalyzed carboacylation of olefins: Ligand-promoted rhodacycle isomerization enables regioselective C-C bond functionalization of benzocyclobutenones. *J. Am. Chem. Soc.* **2015**, *137*, 8274–8283.
12) Lu, G.; Liu, R. Y.; Yang, Y.; Fang, C.; Lambrecht, D. S.; Buchwald, S. L.; Liu, P. Ligand-substrate dispersion facilitates the copper-catalyzed hydroamination of unactivated olefins. *J. Am. Chem. Soc.* **2017**, *139*, 16548–16555.
13) Nozaki, K.; Sakai, N.; Nanno, T.; Higashijima, T.; Mano, S.; Horiuchi, T.; Takaya, H. Highly enantioselective hydroformylation of olefins catalyzed by rhodium(I) complexes of new chiral phosphine-phosphite ligands. *J. Am. Chem. Soc.* **1997**, *119*, 4413–4423.
14) Hu, A.; Ngo, H. L.; Lin, W. Remarkable 4,4′-substituent effects on binap: highly enantioselective Ru catalysts for asymmetric hydrogenation of β-aryl ketoesters and their immobilization in room-temperature ionic liquids. *Angew. Chem., Int. Ed.* **2004**, *43*, 2501–2504.
15) Cardoso, F. S. P.; Abboud, K. A.; Aponick, A. Design, preparation, and implementation of an imidazole-based chiral biaryl P,N-ligand for asymmetric catalysis. *J. Am. Chem. Soc.* **2013**, *135*, 14548–14551.
16) Kean, Z. S.; Akbulatov, S.; Tian, Y.; Widenhoefer, R. A.; Boulatov, R.; Craig, S. L. Photomechanical actuation of ligand geometry in enantioselective catalysis. *Angew. Chem., Int. Ed.* **2014**, *53*, 14508–14511.
17) Pizzolato, S. F.; Štacko, P.; Kistemaker, J. C. M.; van Leeuwen, T.; Feringa, B. L. Phosphoramidite-based photoresponsive ligands displaying multifold transfer of chirality in dynamic enantioselective metal catalysis. *Nat. Catal.* **2020**, *3*, 488–496.
18) Iwamoto, H.; Ozawa, Y.; Takenouchi, Y. Imamoto, T.; Ito, H. Backbone-modified C_2-symmetrical chiral bisphosphine TMS-QuinoxP*: Asymmetric borylation of racemic allyl electrophiles. *J. Am. Chem. Soc.* **2021**, *143*, 6413–6422.
19) Hoge, G.; Wu, T.-P.; Kissel, W. S.; Pflum, D. A.; Greene, D. J.; Bao, J. Highly selective asymmetric hydrogenation using a three hindered quadrant bisphosphine rhodium catalyst. *J. Am. Chem. Soc.* **2004**, *126*, 5966–5967.
20) Zhang, Z.; Tamura, K.; Mayama, D.; Sugiya, M.; Imamoto, T. Three-hindered quadrant phosphine ligands with an aromatic ring backbone for the rhodium-catalyzed asymmetric hydrogenation of functionalized alkenes. *J. Org. Chem.* **2012**, *77*, 4184–4188.
21) Iwamoto, H.; Imamoto, T.; Ito, H. Computational design of high-performance ligand for enantioselective Markovnikov hydroboration of aliphatic terminal alkenes. *Nat. Commun.* **2018**, *9*, 2290.
22) Iwamoto, H.; Endo, K.; Ozawa, Y.; Watanabe, Y.; Kubota, K.; Imamoto, T.; Ito, H. Copper(I)-catalyzed enantioconvergent borylation of racemic benzyl chlorides enabled by quadrant-by-quadrant

structure modification of chiral bisphosphine ligands. *Angew. Chem., Int. Ed.* **2019**, *58*, 11112–11117.
23) Sawatsugawa, Y.; Tamura, K.; Sano, N.; Imamoto, T. A bulky three-hindered quadrant bisphosphine ligand: Synthesis and application in rhodium-catalyzed asymmetric hydrogenation of functionalized alkenes. *Org. Lett.* **2019**, *21*, 8874–8878.
24) Liebman, J. F.; Greenberg, A. A Survey of strained organic molecules. *Chem. Rev.* **1976**, *76*, 311–365.
25) Reissig, H. U.; Zimmer, R. Donor–acceptor-substituted cyclopropane derivatives and their application in organic synthesis. *Chem. Rev.* **2003**, *103*, 1151–1196.
26) Talele, T. T. The "cyclopropyl fragment" is a versatile player that frequently appears in preclinical/clinical drug molecules. *J. Med. Chem.* **2016**, *59*, 8712–8756.
27) Lebel, H.; Marcoux, J. F.; Molinaro, C.; Charette, A. B. Stereoselective cyclopropanation reactions. *Chem. Rev.* **2003**, *103*, 977–1050.
28) Rubin, M.; Rubina, M.; Gevorgyan, V. Transition metal chemistry of cyclopropenes and cyclopropanes. *Chem. Rev.* **2007**, *107*, 3117–3179.
29) Ebner, C.; Carreira, E. M. Cyclopropanation strategies in recent total syntheses. *Chem. Rev.* **2017**, *117*, 11651–11679.
30) Dian, L.; Marek, I. Asymmetric preparation of polysubstituted cyclopropanes based on direct functionalization of achiral three-membered carbocycles. *Chem. Rev.* **2018**, *118*, 8415–8434.
31) Uchida, T.; Irie, R.; Katsuki, T. Chiral (ON)Ru-salen catalyzed cyclopropanation: High *cis*- and enantio-selectivity. *Synlett* **1999**, *3*, 1163–1165.
32) Bonaccorsi, C.; Mezzetti, A. Optimization or breakthrough? The first highly *cis*- and enantioselective asymmetric cyclopropanation of 1-octene by "electronic and counterion" tuning of $[RuCl(PNNP)]^+$ catalysts. *Organometallics* **2005**, *24*, 4953–4960.
33) Johansson, M. J.; Gorin, D. J.; Staben, S. T.; Toste, F. D. Gold(I)-catalyzed stereoselective olefin cyclopropanation. *J. Am. Chem. Soc.* **2005**, *127*, 18002–18003.
34) Kanchiku, S.; Suematsu, H.; Matsumoto, K.; Uchida, T.; Katsuki, T. Construction of an aryliridium-salen complex for highly *cis*- and enantioselective cyclopropanations. *Angew. Chem., Int. Ed.* **2007**, *46*, 3889–3891.
35) Suematsu, H.; Kanchiku, S.; Uchida, T.; Katsuki, T. Construction of aryliridium-salen complexes: Enantio- and *cis*-selective cyclopropanation of conjugated and nonconjugated olefins. *J. Am. Chem. Soc.* **2008**, *130*, 10327–10337.
36) Knight, A. M.; Kan, S. B. J.; Lewis, R. D.; Brandenberg, O. F.; Chen, K.; Arnold, F. H. Diverse engineered heme proteins enable stereodivergent cyclopropanation of unactivated alkenes. *ACS Cent. Sci.* **2018**, *4*, 372–377.
37) Ito, H.; Kosaka, Y.; Nonoyama, K.; Sasaki, Y.; Sawamura, M. Synthesis of optically active boron-silicon bifunctional cyclopropane derivatives through enantioselective copper(I)-catalyzed reaction of allylic carbonates with a diboron derivative. *Angew. Chem., Int. Ed.* **2008**, *47*, 7424–7427.
38) *Boronic acids: Preparation and applications in organic synthesis, medicine and materials*, 2nd revised ed.; Hall, D. G., Ed.; Wiley-VCH: Weinheim, 2011.
39) Sandford, C.; Aggarwal, V. K. Stereospecific functionalizations and transformations of secondary and tertiary boronic esters. *Chem. Commun.* **2017**, *53*, 5481–5494.
40) Rubina, M.; Rubin, M.; Gevorgyan, V. Catalytic enantioselective hydroboration of cyclopropenes. *J. Am. Chem. Soc.* **2003**, *125*, 7198–7199.
41) Zhong, C.; Kunii, S.; Kosaka, Y.; Sawamura, M.; Ito, H. Enantioselective synthesis of *trans*-aryl- and -heteroaryl-substituted cyclopropylboronates by copper(I)-catalyzed reactions of allylic phosphates with a diboron derivative. *J. Am. Chem. Soc.* **2010**, *132*, 11440–11442.
42) Lin, H.; Pei, W.; Wang, H.; Houk, K. N.; Krauss, I. J. Enantioselective homocrotylboration of aliphatic aldehydes. *J. Am. Chem. Soc.* **2013**, *135*, 82–85.
43) Parra, A.; Amenos, L.; Guisan-Ceinos, M.; Lopez, A.; Ruano, J. L. G.; Tortosa, M. Copper-catalyzed diastereo- and enantioselective desymmetrization of cyclopropenes: synthesis of cyclopropylboronates. *J. Am. Chem. Soc.* **2014**, *136*, 15833–15836.
44) Benoit, G.; Charette, A. B. Diastereoselective borocyclopropanation of allylic ethers using a boromethylzinc carbenoid. *J. Am. Chem. Soc.* **2017**, *139*, 1364–1367.
45) Wittmann, B. J.; Knight, A. M.; Hofstra, J. L.; Reisman, S. E.; Jennifer Kan, S. B.; Arnold, F. H. Diversity-oriented enzymatic synthesis of cyclopropane building blocks. *ACS Catal.* **2020**, *10*, 7112–7116.
46) Shintani, R.; Fujie, R.; Takeda, M.; Nozaki, K. Silylative cyclopropanation of allyl phosphates with silylboronates. *Angew. Chem., Int. Ed.* **2014**, *53*, 6546–6549.
47) Zhang, L.; Oestreich, M. Copper-catalyzed enantio- and diastereoselective addition of silicon nucleophiles to 3,3-disubstituted cyclopropenes. *Chem. Eur. J.* **2019**, *25*, 14304–14307.
48) Amenós, L.; Trulli, L.; Nóvoa, L.; Parra, A.; Tortosa, M. Stereospecific synthesis of α-hydroxy-cyclopropylboronates from allylic epoxides. *Angew. Chem., Int. Ed.* **2019**, *58*, 3188–3192.
49) Wu, F. P.; Luo, X.; Radius, U.; Marder, T. B.; Wu, X. F. Copper-catalyzed synthesis of stereodefined cyclopropyl bis(boronates) from alkenes with CO as the C1 source. *J. Am. Chem. Soc.* **2020**, *142*, 14074–14079.
50) Nafe, J.; Herbert, S.; Auras, F.; Karaghiosoff, K.; Bein, T.; Knochel, P. Functionalization of quinoxalines by using TMP bases: Preparation of tetracyclic heterocycles with high photoluminescene quantum yields. *Chem. Eur. J.* **2015**, *21*, 1102–1107.
51) Our attempts to structurally analyze the corresponding copper(I) chloride complexes were unsuccessful; therefore, the detailed structures of the ligands are discussed using the corresponding palladium(II) complexes.
52) The DFT calculations on transition state $\mathbf{TS1}_{allyl}$ for allylchloride (*E*)-**1ec**, which provides allylboronate **4e**, indicated that the addition of borylcopper(I) **I** and the elimination of the chloride occurred in a concerted fashion. This is different from the mechanism of the allylic borylation of allylcarbonates, which proceeds via the formation of an alkylcopper(I) intermediate followed by the β-elimination; for details, see ref. 18.
53) The detailed DFT calculation of whole reaction pathways with (*R*)-**L1** and (*R*)-**L2** are shown in Figure S15 and S17.
54) Contreras-García, J.; Johnson, E. R.; Keinan, S.; Chaudret, R.; Piquemal, J. P.; Beratan, D. N.; Yang, W. NCIPLOT: A program for plotting noncovalent interaction regions. *J. Chem. Theory Comput.* **2011**, *7*, 625–632.
55) Brinkman, E. A.; Berger, S.; Brauman, J. I. α-Silyl-substituent stabilization of carbanions and silyl anions. *J. Am. Chem. Soc.* **1994**, *116*, 8304–8310.
56) Ito, H.; Toyoda, T.; Sawamura, M. Stereospecific synthesis of cyclobutylboronates through copper(I)-catalyzed reaction of homoallylic sulfonates and a diboron derivative. *J. Am. Chem. Soc.* **2010**, *132*, 5990–5992.
57) Iwamoto, H.; Hayashi, Y.; Ozawa, Y.; Ito, H. Silyl-group-directed linear-selective allylation of carbonyl compounds with trisubstituted allylboronates using a copper(I) catalyst. *ACS Catal.* **2020**, *10*, 2471–2476.
58) Falivene, L.; Credendino, R.; Poater, A.; Petta, A.; Serra, L.; Oliva, R.; Scarano, V.; Cavallo, L. SambVca 2. A web tool for analyzing catalytic pockets with topographic steric maps. *Organometallics* **2016**, *35*, 2286–2293.
59) Falivene, L.; Cao, Z.; Petta, A.; Serra, L.; Poater, A.; Oliva, R.; Scarano, V.; Cavallo, L. Towards the online computer-aided design of catalytic pockets. *Nat. Chem.* **2019**, *11*, 872–879.
60) A distortion-interaction-energy analysis (DIA) corroborated that the steric destabilization of the TS structures for the minor products by the silyl modulators on the ligand backbone can be expected to be of crucial importance for the improvement of the selectivities (Figures S23 and S24); for details, see: Bickelhaupt, F. M.; Houk, K. N. Analyzing reaction rates with the

distortion/interaction-activation strain model. *Angew. Chem., Int. Ed.* **2017**, *56*, 10070–10086.
61) The DFT calculations on the intramolecular cyclization step via **TS2** with the backbone-modified ligand (*R*)-**L2** showed identical results, i.e., both stereo-retentive cyclizations **TS2′**$_{major(cis)}$ and **TS2′**$_{minor(cis)}$ are more favorable than those of the stereo-inversive cyclization **TS2′**$_{major(trans)}$ and **TS2′**$_{minor(trans)}$, respectively; for details, see Figures S17 and S26.
62) The activation energy barriers ($\Delta G^{\ddagger}$) of **TS2**s were calculated based on the most stable state of the alkylcopper(I) conformers **III**s under equilibrium; i.e., $\Delta G^{\ddagger}$ of **TS2**$_{major(cis)}$ and **TS2**$_{major(trans)}$ was calculated based on ΔG of **III**$_{major(trans)}$, $\Delta G^{\ddagger}$ of **TS2**$_{minor(cis)}$ and **TS2**$_{minor(trans)}$ was calculated based on ΔG of **III**$_{minor(trans)}$.
63) Laitar, D. S.; Tsui, E. Y.; Sadighi, J. P. Copper(I) β-boroalkyls from alkene insertion: isolation and rearrangement. *Organometallics* **2006**, *25*, 2405–2408.
64) Lee, J.; Radomkit, S.; Torker, S.; Pozo, J.; Hoveyda, A. H. Mechanism-based enhancement of scope and enantioselectivity for reactions involving a copper-substituted dtereogenic carbon centre. *Nat. Chem.* **2018**, *10*, 99–108.
65) Ozawa, Y.; Iwamoto, H.; Ito, H. Stereoselective intramolecular alkylboration of terminal allenes: via allylcopper(I) isomerization. *Chem. Commun.* **2018**, *54*, 4991–4994.
66) Recently, Popp and co-workers have discussed the stereochemistry of carbon centers attached to copper(I) at the benzylic position in their mechanistic study of a copper(I)-catalyzed boracarboxylation; for details, see: Baughman, N. N.; Akhmedov, N. G.; Petersen, J. L.; Popp, B. V. Experimental and computational analysis of CO_2 addition reactions relevant to copper-catalyzed boracarboxylation of vinyl arenes: Evidence for a phosphine-promoted mechanism, *Organometallics* **2021**, *40*, 23–37.
67) Knizia, G. Intrinsic atomic orbitals: An unbiased bridge between quantum theory and chemical concepts. *J. Chem. Theory Comput.* **2013**, *9*, 4834–4843.
68) Knizia, G.; Klein, J. E. M. N. Electron flow in reaction mechanisms - revealed from first principles. *Angew. Chem., Int. Ed.* **2015**, *54*, 5518–5522.
69) Kim, N.; Widenhoefer, R. A. Formation of cyclopropanes via activation of (γ-methoxy)alkyl gold(I) complexes with Lewis acids. *Organometallics* **2020**, *39*, 3160–3167.

Insert Table of Contents artwork here